TECHNICAL REPORT, CB No.326

$\bar{p}p \to \eta\eta\pi^0$ in flight

D.V. Bugg, QMWC, London œ[Bœ[B

œ[Bœ[B

Feb 8, 1998 œ[B

Abstract

Data on the final state $\eta\eta\pi^0$ in flight are presented for beam momenta 900, 1050, 1350, 1525, 1642, 1800 and 1940 MeV/c. There is direct visual evidence for the presence of a broad high mass 2^+ contribution in $\eta\eta$; the amplitude analysis shows it may be fitted as a resonance with mass $M = 1980 \pm 50$ MeV and width $\Gamma = 500 \pm 100$ MeV. It has the curious feature that it is produced dominantly with orbital angular momentum $L = 1$ in the final state and with z-component of spin 1 along the beam direction. It makes up typically 15–20% of the integrated cross section at 1525 MeV/c and above.

In addition, the presence of $a_2(1660)$ is confirmed at beam momenta from 1350 MeV/c upwards; however, because of the limited phase space in the $\eta\pi$ channel, it is not possible to improve the determination of its mass and width compared with earlier analyses of data at 1940 MeV/c. Its production requires dominant production with $L = 0$ in the final state, i.e. from the initial state $^1D_2$.

The $f_J(2100)$ in $\eta\eta$ is likewise produced with a cross section consistent with dominant $L = 0$ in the final state and is incompatible with much $L = 1$; using this fact and the observed decay angular distribution, it definitely has $J = 0$, in agreement with earlier spin determinations.

1 Introduction

It looks as if we have had a lucky break. Before plunging into detail, I will outline this fortunate result and why we were looking for it.

In an article in Phys. Lett. [1], Bing Song Zou and I described the evidence for a very broad 0^- object in J/Ψ radiative decays to $\rho\rho$, $\omega\omega$, $K^*\bar{K}^*$ and $\phi\phi$. It

has a mass somewhere in the range 1750-2100 MeV and a width $\sim$ 1 GeV. Its decays are flavour blind within experimental errors. Its integrated cross section agrees with the prediction of Close, Farrar and Li [2] for a glueball. Its mixing with the first radial excitation of $\eta'(958)$ can explain the iota $\equiv \eta(1440)$.

We speculated that there will be a similar broad resonance with $J^P = 2^+$ around a mass of 2 GeV. The mixing of this broad state with the first radial excitation of $f_2'(1525)$ could explain the $\theta \equiv f_J(1710)$. Its mixing with further radial excitations could explain the exotic $\phi\phi$ resonances observed by Etkin et al. [3.] from 2020 to 2340 MeV. The reason we proposed a broad state is that it needs to overlap the mass range 1710 to 2340 MeV.

Since then, Anisovich, Sarantsev and I [4] have realised that glueballs will naturally mix with $q\bar{q}$ states to make a broad state containing a dominant glueball component, as observed for 0^+. So a broad 2^+ appears quite natural

The lucky break is that a broad 2^+ state indeed appears in the $\eta\eta\pi$ data in flight. We looked there first because $\eta\eta$ is the obvious channel for a glueball. The broad state is visible by eye in the raw data when one chooses the right angular distribution to plot. Therefore its presence is not dependent on a partial wave analysis, though the amplitude analysis does confirms it and determines the mass and width with reasonable errors. It has the additional feature of very curious helicity properties, strikingly different to the regular $\bar{q}q$ state $a_2(1660)$. That difference and the specific L dependence of the amplitudes suggests non $\bar{q}q$ character; one can make a speculative argument associating $f_2(1980)$ with what is expected of a glueball.

There are probably two further observations of this broad state. The Omega group [5] observes a broad 2^+ enhancement in low p_T central production at a similar mass: M = 1930 MeV and with similar width Γ = 460 MeV. The BES group [6] has presented at Hadron'97 an analysis of their data on $J/\Psi \to \gamma(4\pi)$; that analysis also requires a broad 2^+ signal with similar mass and width; M = 2010 MeV, Γ = 350 MeV.

2 Event Selection and Backgrounds

The event reconstruction follows the standard procedures developed earlier for all-neutral final states in flight. A condensed version of the essential features will be given here. Versions of CBAR software which have been used are:

- CBar General Offline Software Version 1.30/09
- Crystal Data Reconstruction Version 2.04/03
- Global Tracking Version 1.37/01
- CBKFIT Version 3.09/00
- Brain Version 3.03a
- Fast Fuzzy Pattern Recognition.

BCTRAK is not used, since charged particles are not reconstructed, only vetoed. Events with a PED centred in Crystal 13 have NOT been rejected, as has been the practice at rest; it rejects too many events. We rely on overall energy-momentum balance to reject events where photon energy is lost down the beam-pipe.

Data on all final states with 4-10 γ have been examined. All have a total energy peak centred $3 \pm 1\%$ below the nominal total energy. The only explanation we can find is that all photon energies need scaling upwards by 3% and this has been done in the final selection of events. It has rather little effect: differences in selection of events with and without this scaling factor are at the level of 1% of events selected; there is no visible change on the Dalitz plot or projections. After event reconstruction, data are fitted kinematically to 43 channels which were agreed between Bochum and the UK group. Some of these channels turn out to have negligibly few events. However, at least 20,000 Monte Carlo events have been generated for all 43 channels at a beam momentum of 1800 MeV/c. Monte Carlo events from every channel have been fitted to all 43 channels, in order to estimate reconstruction efficiencies (from events fitted to the correct channel) and cross-talk between channels (from events fitted to the wrong channel). Using these Monte Carlo events and data, we are able to estimate (i) the level of cross-talk, (b) the numbers of good events in all channels. This is done by solving a 43 x 43 set of simultaneous equations containing on the left-hand side the observed number of fitted data events, and on the right-hand side reconstruction efficiencies and numbers of events in every channel. The solution is constrained so that the numbers of events in every channel are positive or zero.

We have tried a large number of alternative prescriptions for selecting events. For example, confidence levels were varied and different procedures were tried for handling split-offs and merged pions. It rapidly became clear that the dominant backgrounds in the $\eta\eta\pi$ final state arise from $\omega\pi^0\pi^0$ events ($\omega \to \pi^0\gamma$) where one photon is lost and also $\eta 3\pi^0$ events where two photons are lost. These channels both have quite large branching ratios compared with $\eta\eta\pi$. This made it immediately obvious that it is dangerous to try to recombine split-offs with parent PEDS, since a genuine low energy photon can then get absorbed into a PED and this will make the event look like a 6γ event. Therefore we decided to use only events containing exactly 6 PEDS with photon energies above 20 MeV. Events with split-offs are rejected. For similar reasons, events containing merged π^0 were rejected (i.e. events where two photons from a π^0 produce a single PED). The loss of events from these two decisions is $< 10\%$ and it reduces background levels by a factor 3, from roughly 27% to 7.8%.

The $3\pi^0$ and $\eta\pi^0\pi^0$ channels have branching fractions greater than $\eta\eta\pi^0$ by factors of roughly 30 and 15 respectively. Cross-talk from these channels is reduced to a low level by rejecting events which fit these channels with a confidence level $> 0.1\%$; Joerg Luedemann used a cut at 0.01% confidence level, but the difference in background compared with the 0.1% cut is negligible. Events from 3η are rare, and easily eliminated by rejecting events which fit this channel with confidence level $> 1\%$.

The residual level of backgrounds at 1800 MeV/c is shown in Table 1 for three confidence levels. We decided that the small reduction in background in going from 10% confidence level to 20% was not worth the loss of events.

At other beam momenta, we have simulated by Monte Carlo only the backgrounds shown explicitly in Table 1. Within the available statistics, these backgrounds are roughly linearly proportional to beam momentum. Table 2 summarises statistics and backgrounds. Within the errors, the backgrounds are distributed according to phase space. (The structures visible within the $\omega\pi^0\pi^0$ and $\eta 3\pi^0$ channels are not strong and do not distort the phase space distribution of backgrounds at the level at which we are presently working). In the amplitude analysis reported below, we have included phase space backgrounds of the magnitudes we estimate. Fortunately, they have almost no effect on the physics; when the background is set to zero, log likelihood changes by extremely small amounts, typically 1 or 2. Thus we are confident that these levels of background have negligible effect on physics conclusions.

3 Features of the Data

Figs. 1 and 2 show Dalitz plots for data and the fit and also projections on to $M(\eta\pi)$ and $M(\eta\eta)$. In this report we shall concentrate on the physics to be extracted from the four highest beam momenta: 1350, 1525, 1642 and 1800 MeV/c. These are shown in Fig. 1. The remaining momenta are shown in Fig. 2 for completeness. It has become evident that it is desirable to try to fit both production and decay at the lower momenta; but this is unrealistic with the available statistics at the higher momenta, where many partial waves are required in the $\bar{p}p$ channel. Therefore, in this report we shall concentrate on the physics of the data from 1350 MeV/c upwards. The analysis of the lower momenta must also await processing of data at 1200 and 600 MeV/c.

The features which are immediately obvious by eye are bands on the Dalitz plots due to final states $a_0(980)\eta$, $a_2(1320)\eta$ and $f_0(1500)\pi$. Data on final states of $3\pi^0$ will be reported separately; they were shown at the October 1997 collaboration meeting. They contain a very obvious contribution of roughly 30% from $f_2(1270)\pi$. One can then calculate the expected contribution in the $\eta\eta\pi^0$ final state using the PDG branching ratio of $f_2(1270) \rightarrow \eta\eta$. It comes out to be about 5–7%. This amount is barely visible in $\eta\eta\pi^0$ data by eye, but when added to the fit it does give a significant improvement in log likelihood and fits to roughly the right magnitude. The fit is not sensitive to substituting $f_0(1300)$ for all or some of the $f_2(1270)$ signal. It seems likely that $f_2(1270)$ will dominate strongly over $f_0(1300)$; therefore we omit $f_0(1300)$. The fit is improved slightly by adding some small amount of $f_0(975) \rightarrow \eta\eta$, but this has little effect on any physics conclusions.

As a reminder, data at 1940 MeV/c are shown in Fig. 3. These data have been extensively analysed by Joerg Luedemann and Holger Stoeck. There is a conspicuous enhancement at the bottom left corner of the Dalitz plot where the $a_0(980)$ bands cross. From analyses at 1940 MeV/c, we know that this feature cannot be fitted adequately by the crossing $a_0(980)$ bands alone. It has been necessary to add a resonance $f_J(2120 \pm 25)$ decaying to $\eta\eta$. We include this in the analysis of the present data with the objective of trying to find out whether $J = 0$ or 2. We shall call it $f_J(2100)$, since our conclusion will be that it is consistent with peaks at that mass observed in $J/\Psi \rightarrow \gamma(4\pi)$ [7] and the high statistics E760 experiment at Fermilab [8].

The data of Fig. 2 show enhancements in the $\eta\eta$ channel around 1770 MeV, as discussed below. There is earlier evidence [9] for a spin 0 resonance at this mass. However, it is also possible that the θ meson, $f_J(1710)$ contributes in this

mass range. Disentangling contributions from these two possible contributions turns out to be quite delicate. For present purposes it has almost no impact on the analysis of data at beam momenta 1350–1940 MeV/c. For reasons discussed below, it will need a separate study of beam momenta 600–1350 MeV/c.

4 Amplitude Analysis

Channels fitted to the data are as follows:

$$\begin{aligned}
\bar{p}p &\rightarrow a_0(980)\eta && (1)\\
&\rightarrow a_2(1320)\eta && (2)\\
&\rightarrow a_2(1660)\eta && (3)\\
&\rightarrow f_0(975)\pi && (4)\\
&\rightarrow f_2(1270)\pi && (5)\\
&\rightarrow f_0(1500)\pi && (6)\\
&\rightarrow f_J(2100)\pi \quad or \quad f_4(2050)\pi && (7)\\
&\rightarrow f_2(1980)\pi && (8)\\
&\rightarrow f_0(1770)\pi && (9)\\
&\rightarrow f_J(1710)\pi. && (10)
\end{aligned}$$

Of these, the last two are relevant only at the lower beam momenta. Except for the broad $f_2(1980)$ and the $f_0(1770)$, masses and widths are set to PDG values. There is no significant evidence for departure from these values. For $a_0(980)$, a Flatté formula is used with parameters taken from previous work [10]. We have also tried adding $a_0(1450)$ and an a_0 in the mass range 1650–1800 MeV. There is no significant evidence for either.

4.1 The Wick rotation

There are too many partial waves to fit both production and decay of all channels. We fit the decay process in full, since this gives the primary information on J^P of resonances. Some approximations are needed in treating the production process, which tells us about partial waves contributing from the $\bar{p}p$ channel. The amplitude analysis uses the same general strategy as in the analysis of early data at 1940 MeV/c. The decay for each channel is parametrised by an amplitude

$$f_m = \frac{G_m\ B_J\ Y_J^m(\alpha,\beta)\exp(i\delta)}{M^2 - s - iM\Gamma}. \qquad (11)$$

Here J is the spin of the resonance in each of channels (1)–(10) and m is its component of spin along the beam direction. In Breit-Wigner amplitudes, a constant width Γ is assumed.

The angles α and β are illustrated in Fig. 4. They are the decay angles of the resonance with respect to the beam direction after a Wick rotation. The details of the Wick rotation are given in our paper on $\bar{p}p \to \eta 3\pi^0$ in flight [11]. In outline, the steps are as follows. Particle momenta are transformed from the lab to the centre of mass frame and then rotated through angles τ, ϕ to the direction of production of the final state described by any one of the channels (1)–(10). They are then boosted to the rest frame of the resonance. Then they are rotated back again through angles $-\phi$ and $-\tau$ in the rest frame of the resonance. The effect of the second rotation is to cancel the quantum mechanical rotation matrices required for the first rotation. Amplitudes are invariant under the boost to the rest frame of the resonance. This procedure eliminates the need for rotation matrices. We shall find that the angle α has a further virtue in displaying clearly the broad $f_2(1980)$. The decay of the resonance X into spin 0 particles π and η is described simply by the spherical harmonics $Y_J^m(\alpha, \beta)$. In equn. (11), there is a separate real coupling constant G_m for $m = 0$ and every positive m value. Values of G_m are the same for positive and negative values of m. Interferences between all channels (1)–(10) are examined. The ones which are kept in the final fit are those where log likelihood improves by more than 2 $\times$ the number of m values, i.e. at least a 2 standard deviation effect.

The initial $\bar{p}p$ state can have a component of spin along the beam direction of 1, 0 or -1. Therefore formation of a resonance with $m = \pm 2$ requires a transfer of at least one unit of orbital angular momentum between initial and final states. This implies a factor $\sin\tau$ in the amplitude of equn. (11). Likewise, resonances with $m = \pm 3$ or ± 4 requires factors $\sin^2\tau$ or $\sin^3\tau$. These factors are included by multiplying them into equn. (11). However, this point is academic, since all amplitudes with $m > 1$ optimise at zero. It is general experience from previous experiments (e.g. the CERN-Munich [12] experiment) that amplitudes with $|m| > 1$ are strongly suppressed. We find the same result in the present analysis. This makes a considerable simplification. In the previous analysis [11] by Andy Cooper of $\eta 3\pi^0$ data in flight, all amplitudes with $|m| > 1$ were also small, though they were not actually set to zero.

5 Choice of amplitudes for each channel

We now discuss details of each individual channel (1)–(10). Here one must be clear about our essential objectives in order to understand what approximations are reasonable. The objectives are: (a) to distinguish between $J = 0$, 2 and 4 for $f_J(2100)$, (B) to fit $f_2(1980)$, and (C) to confirm $a_2(1660)$. Consider first $f_J(2100)$. At a beam momentum of 1940 MeV/c, it is produced with a mean centre of mass momentum of $k = 256$ MeV/c. At lower beam momentum, k is even smaller. A useful rule-of thumb from earlier experience is that 250 MeV/c is required for each unit of orbital angular momentum L in the final state. This rule of thumb may be compared with predictions from Blatt-Weisskopf factors B_L given below, using a radius of interaction $R = 0.8$ fm. For $L = 1$, $B_1 = 0.7$ and for $L = 2$, $B_2 = 0.26$; these factors multiply the *amplitude*.

We therefore fit the production and decay of $f_J(2100)$ in full with $L = 0$ and 1 only. ($L = 2$ has been tried, but makes negligible contribution.) For $J = 0$, this means production from $^1S_0$ and $^3P_1$ initial states; the latter contributes only to $m' = 1$ because the Clebsch-Gordan coefficient for $m' = 0$ is zero. (Here m' is the helicity in the *initial* state). For $J = 2$, $L = 0$ requires the initial state $^1D_2$; for $L = 1$, there are four amplitudes: $^3P_1$, $^3P_2$, $^3F_2$ and $^3F_3$, each with its own phase δ. For $J = 4$, the corresponding states are $^1G_4$ for $L = 0$ and $^3F_3$, $^3F_4$, $^3H_4$ and $^3H_5$ for $L = 1$. Earlier experience in fitting $\bar{p}p \to \pi^-\pi^+$ [13] is that H-waves make very small contributions even at 1940 MeV/c, because of the strong centrifugal barrier in the $\bar{p}p$ entrance channel.

Next consider $a_0(980)\eta$. Its interferences with $f_J(2100)$ play an important role, particularly at 1940 MeV/c. There $k \simeq 1$ GeV/c. We fit all partial waves explicitly up to $L = 3$; $L = 4$ is barely significant and tends to produce instability in the fit.

Production and decay of $f_0(1500)$ may be treated likewise, but in practice has little effect on the fit. At all beam momenta its production angular distribution is isotropic within errors. In order to keep the fit as simple as possible, we therefore treat it with a single amplitude, independent of τ.

Production of $a_2(1320)$ has to be treated in an approximate way. At a beam momentum of 1940 MeV/c, $k = 720$ MeV/c. Consider as an example, what would be involved for $L = 2$. A full parametrisation would require the inclusion of $^1G_4$, $^3F_3$, $^3F_2$, $^1D_2$ (both $L = 0$ and $L = 2$), $^3P_2$, $^3P_1$ and $^1S_0$ initial states. There are not enough data to support this possibility and for $L = 3$ there are five more partial waves. We find that $a_2(1320)$ is produced with some slight $\cos\tau$

dependence. We allow for this τ dependence in an approximate way by allowing these amplitudes to be multiplied by a factor $F(\tau) = 1 + \gamma \cos^2\theta$. [Only even powers are allowed by charge conjugation invariance, since the spectator η does not distinguish between incident $\bar{p}$ and p]. The factor γ is optimised numerically, and is typically 0.3. We have tried adding terms involving $\cos^4\tau$, but these do not improve the fit significantly. We find that production of $a_2(1650)$ is consistent with dominant $L = 0$ at all beam momenta; that result is slightly surprising since k = 405 MeV/c at a beam momentum of 1940 MeV/c. Nonetheless we take advantage, and fit simply with $m = 0$ and $m = 1$ amplitudes; the latter is almost negligible, improving log likelihood at most by 5 per momentum.

6 Cross sections and Interferences

Contributions to the cross section from $a_0(980)$ and $f_J(2100)$ are calculated fully from the sums of singlet (L = 0 and 2) and triplet (L = 1 and 3, m = 0 and 1) cross sections. Other channels contribute the modulus squared of each helicity amplitude,. Interferences between channels need to be handled approximately. Consider $a_2(1320)$ interfering with $f_0(1500)$ as an example. Let their amplitudes be A and B for $m = 0$. Each is presumably produced from many initial $\bar{p}p$ states. The interference terms are therefore fitted as $cRe(A^*B)$, where c is a coherence factor fitted in the range -1 to +1, and allowing for partial coherence between A and B. The interference of the two crossing $a_2(1320)$ bands is treated likewise. In practice these interferences are significant only where bands cross in the Dalitz plot. Except for $a_0(980)$ crossing $f_J(2100)$, they play little role in extracting physics; the $a_0(980)$ interference with $f_J(2100)$ is treated exactly.

6.1 Centrifugal Barrier factors

For the decay of $f_2(1270)$ to $\eta\eta$, a centrifugal barrier for decay B_2 is included using the standard Blatt-Weisskopf form:

$$B_2 \propto \frac{3k^2R^2}{[1 + 3k^2R^2(1 + 3k^2R^2)]^{1/2}}. \tag{12}$$

This has only a small effect. Other resonances are far from threshold and the effect of the centrifugal barrier is negligible. In equn. (12), k is the decay momentum. For production of $f_2(2100)$, we include a standard Blatt-Weisskopf centrifugal barrier for production via partial waves having $L = 1$:

$$B_1 \propto \frac{kR}{[1 + k^2R^2]^{1/2}}. \tag{13}$$

6.2 Definition of log likelihood

Log likelihood, S, is defined as follows:

$$S = (\sum_{j=1}^{N} \ln w_j) - N \ln(\sum_{i=1}^{M} w_i). \tag{14}$$

Here N is the number of data events, M is the number of Monte Carlo events, and w is the cross section for the kinematics of a particular event. With this definition, a change of log likelihood of 0.5 corresponds to 1 standard deviation. The sign of log likelihood is such that the optimum fit is given by the most negative value.

6.3 Normalisation

Cross sections are obtained from the number of reconstructed events, corrected for efficiency as determined from the Monte Carlo simulation; the normalisation is done with respect to beam counts used in the primary trigger. This is defined by a coincidence between Ken's chamber and the OR of the SiLi counters. The beam counts are corrected to the livetime of the data-recording system using two clocks, one of which runs continuously, as does the beam scaler; the second clock is gated off when the data-recodring system is busy. We have checked that the measured cross section is independent of beam rate to better than 1%.

At the present stage, no attempt is made to obtain an absolute normalisation. Arbitrarily, we choose to normalise against a fixed number of beam counts, For present purposes, only relative cross sections at different beam momenta are needed. Table 3 shows the number of $\eta\eta\pi^0$ events (corrected for efficiency) per 10^8 $\bar{p}$.

7 The broad $f_2(1980) \to \eta\eta$

In fitting data at 1940 MeV/c, both Joerg Luedemann and Holger Stoeck found that a high mass contribution with $J = 2$ in the $\eta\eta$ channel improved log likelihood. They both sought to identify it with $f_J(2100)$. However, this was always a doubtful identification. That resonance is rather narrow, and most of the improvement in log likelihood did not come from the peak region. If the low mass tail of this resonance below 2000 MeV was excluded from the fit, log likelihood was very similar using $f_2(2120)$ or $f_0(2120)$; it differed only by 8. At the collaboration meeting in July 1997, I demonstrated that the best fit to the data was obtained with $f_0(2120)$ and a broad 2^+ contribution.

We no longer need to rely on the amplitude analysis to demonstrate the presence of the broad 2^+. With the right choice of plot, it is obvious by eye. At all beam momenta, the production angular distribution for $\eta\eta$ final states is independent of production angle θ within errors. This is illustrated for one beam momentum in Fig. 5. In order to examine the spin of the $\eta\eta$ system, one can then plot distributions against either $\cos\alpha$ of Fig. 4 or $\cos\alpha'$. The angle α is that for decay products of the resonance measured with respect to the beam direction, after the Wick rotation; the angle α' is measured instead with respect to the direction of the resonance. The angle α' has a disadvantage. It is a well know result that $\cos\alpha'$ varies linearly along a band in the Dalitz plot. When another resonance band crosses, it shows up as a strong perturbation of the distribution against $\cos\alpha'$. If one uses instead $\cos\alpha$, this feature disappears, since it is smeared out by the relation $\alpha = \theta + \alpha'$ after averaging over τ. The observed absence of $\cos\tau$ dependence means that it does not matter whether one plots against $\cos\alpha$ or $\cos\alpha'$.

Fig. 6 shows the dependence of data on $\cos\alpha$ for a beam momentum of 1350 MeV/c. This beam momentum has been chosen so that $a_2(1320)$ bands lie outside the range of $\eta\eta$ masses being plotted. The mass range barely extends beyond 2 GeV, so Fig. 6(h) shows masses above 2 GeV for the highest beam momentum of 1940 MeV/c. Results for other beam momenta are similar, and Fig. 7 shows the dependence on $\cos\alpha$ at 1525 MeV/c; here all panels refer to this momentum. For the $f_0(1500)$ band, the data are flat, consistent with the expected spin 0. (Any contribution from $f_2'(1525)$ must be small, since it fails to fit either the mass or the width of the peak in $\eta\eta$; we also know it to be small from $K^+K^-\pi^0$ data of Michael Ratajczak at 1940 MeV/c). For $\eta\eta$ masses above 1550 MeV, the distributions against $\cos\alpha$ are far from flat. That requires a contribution from $J \geq 2$. One does not expect $J = 4$ until close to $M_{\eta\eta} = 2040$ MeV; also, from data on $\bar{p}p \to \pi^-\pi^+$, it is known that $f_4(2040)$ is produced only weakly, so it seems unlikely to account for the features of Figs. 6 and 7. We shall show below that fits with $J = 4$ are considerably worse than with $J = 2$.

From Figs. 6 and 7, we can immediately deduce a very curious property of the broad 2^+ contribution. This feature is so curious that I have searched long and hard to make sure there is no error in the (very simple) programme! It is dominated strongly by production with $m = \pm 1$. The amplitude with spin component m along the beam is proportional to $P_2^m(\cos\alpha)$. Remember that

$$P_2^0 \propto (1.5\cos^2\alpha - 0.5), \tag{15}$$

$$P_2^1 \propto \cos\alpha\sin\alpha, \tag{16}$$

$$P_2^2 \quad \propto \quad \sin^2\alpha. \tag{17}$$

In Fig. 6, it is obvious that the contribution from P_2^2 must be small, since the data tend to small values at $\cos\alpha = 0$. The contribution from P_2^0 has a zero at $\cos\alpha = 1/\sqrt{3}$; there is no sign of this in the data. The data peak around $\cos\alpha = 1/\sqrt{2}$, which is where P_2^1 peaks. So it is obvious that the amplitude with $m = \pm 1$ dominates. The amplitude analysis confirms this.

7.1 Amplitude Analysis

The amplitude analysis has been done in two ways, and both give very similar results. Firstly the $f_2(1980)$ contribution has been fitted, like $f_2(1270)$ and $a_2(1320)$, with three amplitudes having $m = 0$, ± 1 and ± 2. As usual, the component with $m = 2$ optimises at zero. The component with $m = 1$ dominates by a factor ~ 10 in cross section over $m = 0$.

The second method of fitting derives historically from the way the programme was written to fit $f_J(2100)$. Both production and decay are fitted assuming $L = 0$ or 1 in the final state. The fitted partial waves are then $^1D_2$ ($L = 0$), and $^3P_1$, $^3P_2$, $^3F_2$ and $^3F_3$ (the last four with $L = 1$). This method has the virtue of displaying the relative contributions of $L = 0$ and the contributions with $L = 1$. What emerges is that the $L = 0$ contribution is surprisingly small at all beam momenta. The reason is that it requires $m = 0$ and the P_2^0 amplitude does not fit the data. The $L = 1$ contributions are all significant and somehow conspire to produce a dominant $m = 1$ amplitude.

I have checked the sensitivity of the fit to individual contributions from $^1D_2$, $^3P_1$, $^3P_2$, $^3F_2$ and $^3F_3$ by varying the magnitudes of each in turn, re-optimising all other amplitudes and all phases. What emerges is that contributions from the five amplitudes $^1D_2$, $^3P_1$, $^3F_3$ and the 2^+ amplitudes with initial helicites $m' = 0$ and 1 are well separated by their specific angular dependences. Much of the cross section producing the broad $f_0(1980)$ comes from the initial 2^+ state with helicity $m' = 0$. Clebsch-Gordan coefficients are such that this amplitude leads to purely $m = \pm 1$ final states. Contributions from 2^+ initial states with $m' = 1$ are almost absent. The remaining cross section comes almost entirely from initial states $^3P_1$ and $3F_3$; their relative magnitudes and phases conspire with the small 2^+ $m' = 1$ amplitude to produce final states which are dominantly $m = 1$. Contributions from the initial state $^1D_2$ ($L = 0$ in the final state) are surprisingly small: everywhere $< 15\%$ of the cross section for the broad $f_2(1980)$, and frequently only 5%. In view of the centrifugal barrier hindering $L = 1$ final states, that is very surprising.

This result is in striking contrast to the behaviour of $a_2(1660)$, which will be discussed in detail below. It is dominated at all momenta by the final state with $m = 0$. Its production cross section versus momentum k in the final states is consistent with $L = 0$ if one allows for some saturation as the momentum rises; this is shown in Fig. 8.

For $f_2(1980)$, the dominance of $L = 1$ offers a strong hint that the broad 2^+ has a large glueball component. According to Isgur et al., a confined gluon is not a gluon in its ground state, but is excited with a component $L = 1$ along a direction about which it rotates. They have shown that hybrids should decay preferentially to $\bar{q}q$ states containing $L = 1$ between the quarks. This implies that the excited gluon cannot readily transfer its orbital angular momentum to the spin of the quarks, because the spin-orbit interaction is too weak. It is plausible that the same will be true for two gluons in a glueball. If one views the process $\bar{p}p \to \pi(gg)$ in reverse as a virtual decay of the glueball, there should be a preference for producing a pion with $L = 1$ and a $\bar{p}p$ system with internal $L = 1$. That would be consistent with the observed strong dominance of $L = 1$ over $L = 0$. The argument is however incomplete, since Table 3 shows that the $^3F_3$ partial wave with $\ell_{\bar{p}p} = 3$ is stronger than $^3P_1$ with $\ell_{\bar{p}p} = 1$. The argument also fails to explain why $m = 1$ dominates.

Regardless of these conjectures, Fig. 6 makes it quite obvious that the broad 2^+ object is present. To optimise its mass M and width Γ, the following procedure was adopted. The entire fit was made at each momentum for a grid of values of M from 1850 to 2100 MeV in steps of 50 MeV and Γ from 300 to 600 MeV in steps of 50 MeV. Values of log likelihood were added from fits to data at 5 momenta from 1350 to 1940 MeV/c. The optimum is at $M = 1980$ MeV, $\Gamma = 500$ MeV. This is illustrated in Fig. 9. However, it is likely to be an approximation to use a constant width. The $\rho\rho$ and $\omega\omega$ channels are opening rapidly from 1550 MeV and $K^*\bar{K}^*$ opens at 1780 MeV. Our experience in fitting the broad $0^-(1750-2100)$ is that opening of these channels and the s dependence of the width may play quite a strong role. From the present data, there is some indication of this. The data at 1350 MeV/c optimise at $M = 1900$ MeV, those at 1525 MeV/c at $M = 1940$ MeV and with increasing beam momentum the optimum mass gradually increase to 2020 MeV; as the mass increases, the fitted Γ increases gradually from 400 to 590 MeV. A reasonable compromise amongst these results is $M = 1980 \pm 50$ MeV, $\Gamma = 400$–600 MeV.

8 $a_2(1660)$

Earlier work at 1940 MeV/c, with which I agree, has shown a clear optimum for this resonance at $M = 1660 \pm 15(stat) \pm 15(syst)$ MeV, $\Gamma = 280 \pm 30 \pm 30$ MeV. The key feature which identifies it is the constructive interference between the two $a_2(1660)$ bands at the right-hand edge of the Dalitz plot. This is illustrated in Fig. 10. The $m = 0$ amplitude is completely dominant. It has an angular dependence $P_2^0(\cos\alpha)$, which peaks at each end of the band, where $\cos\alpha = \pm 1$. Constructive interference between the two bands in the $m = 0$ amplitude is responsible for the enhancement at the right-hand edge of the Dalitz plot.

There is a strong requirement for $a_2(1660)$ at all beam momenta from 1350 to 1940 MeV/c. Typically it improves log likelihood by 50–70. Detailed numbers for this channel and others are given in Table 6.

However, $a_2(1660)$ lies towards the top end of the available $\eta\pi$ phase space. In consequence, data below 1940 MeV/c do not improve the determination of its mass and width. As these are varied, log likelihood gets rapidly worse as M is decreased below 1630 MeV, so this is a safe lower limit on the mass. But for masses above 1700 MeV, log likelihood flattens off and Γ increases. One cannot see a real optimum. The VES group presented data at Hadron'97 showing an $a_2(1700)$ decaying to $\rho\omega$ [15].

9 $f_J(2100)$

I begin by reviewing results from earlier work at 1940 MeV/c. Joerg Ludedmann and Holger Stoeck have not included the broad $f_2(1980)$ and have used only a single resonance which optimises in the mass range 2120 to 2160 MeV, depending on the choice of J. However, it was always clear that most of the preference for $J = 2$ (or 4) arose from the mass range below 2000 MeV. When the amplitude was cut off below that mass, all J gave fits of similar quality.

There was a second disturbing feature. One expects the centrifugal barrier to suppress the $L = 1$ cross section by at least a factor 2 compared with $L = 0$. If $J = 2$, allowing for multiplicies available to the various partial waves, one anticipates that the $^1D_2$ cross section ($L = 0$) should be roughly similar in magnitude to the sum of $L = 1$ cross sections from $^3P_1$, $^3P_2$, $^3F_2$ and $^3F_3$. But the fits gave a very different picture. Results of my fits are summarised in Table 5.

Let us start from a reference fit without $f_J(2100)$. Since the zero of log like-

lihood is arbitrary, I define this as the zero. If one adds a $J = 0$ resonance with only $L = 0$ and optimises its mass and width, log likelihood immediately improves spectacularly by 96.1 (entry 2 of Table 5). Adding $L = 1$ from $^3P_1$ has very little further effect (entry 3).

Next consider $J = 2$. With only $L = 0$ ($^1D_2$), entry 5, log likelihood is much worse than for $J = 0$. The reason is that the decay angular distribution is completely incompatible with $|Y_2^0(\alpha)|^2$. However, adding $L = 1$ production from $^3P_1$, $^3P_2$, $^3P_2$ and $^3F_3$ allows a good fit to both production and decay, entry 6 of Table 5. With hindsight, this is obviously helping to fit the broad $f_2(1980)$ contribution. œ Next consider $J = 4$. The story is very similar to $J = 2$. Distinguishing between these two possibilities is hindered by the drop in acceptance near the beam direction, $\cos\alpha = \pm 1$. The $L = 0$ contribution alone, entry 7, gives a poor fit, even if M and Γ are fitted freely. The reason is that $|Y_4^0(\alpha)|^2$ fails to fit the decay angular distribution. However, again adding $L = 1$ production from $^3F_3$, $^3F_4$, $^3H_4$ and $^3H_5$ allows a good fit to both production and decay, entry 8. The $J = 4$ fit is able to fit wiggles in the data which could easily arise from statistical fluctuations.

A $J = 4$ contribution seems likely to come from $f_4(2050)$; if we fix M, Γ at PDG values, log likelihood is decidedly worse, namely 116.1.

Entry 4 shows a fit including the broad $f_2(1980)$ and $f_0(2104)$ with $\Gamma = 216$ MeV and only $L = 0$. The mass and width have been fixed at values from expt E760 at Fermilab. This experiment has by far the highest statistics, and shows an exceedingly strong peak in $\eta\eta$.

Table 5, entry 6, shows that $f_2(2120)$ including $L = 1$ is capable of fitting the data, but with a remarkably small $L = 0$ contribution. If this fit is to be believed, the production cross section should show a k^3 dependence on the centre of mass momentum k of the resonance. Strictly speaking, this will be modified to $k^3/(k^2 + 0.0608)$ with k in Gev/c by the centrifugal barrier factor $(B_1)^2$; but in practice the effect of B_1 is small, because $k^2 < 0.0608$. On the other hand, if $J = 0$, the cross section will be proportional to k, with perhaps some form factor attenuating the cross section for large k. Fig. 11 shows the cross section for $f_2(2100)$ as a function of k. Both curves are drawn arbitrarily through the point at 1800 MeV/c as a guide. The full line is linear in k, corresponding to $L = 0$ production; the dashed curve refers to $L = 1$ production. It obviously fits much better to $L = 0$, hence $J = 0$, though there is an obvious indication that the cross section is saturating as the momentum rises. If one fits with $J = 0$, the cross section is almost indistinguishable from that of Fig. 11.

If one persists in fitting with $J = 2$, the decay angular distribution at 1940 MeV/c, calculated from the fit, is isotropic within errors.

Much of the discussion presented so far in this section has arisen because it was necessary to challenge the conclusion of Joerg Luedemann that $J = 2$ is statistically better than $J = 0$. Once the broad 2^+ component has been recognised, it is in fact straightforward to insert into the fit one broad component with spin 2 and a second narrow one with J = 0 or 2 or 4. This procedure leads immediately to a well defined optimum choosing J = 0 for $f_J(2100)$ and optimising the masses and widths of the two contributions. The latter than optimises at 2115 MeV with a width of 210 MeV. These results are consistent within errors with results of the E760 group, but the latter are statistically superior.

In summary, the conclusion is that $J = 0$ from (i) a strong isotropic contribution to production, Fig. 6(h), (ii) a flat decay angular distribution, and (iii) the k dependence of the production cross section, Fig. 11. This result agrees with the J^P analysis of $J/\Psi \to \gamma(4\pi)$ [8]. The strong peak in E760 data has never been properly analysed, mainly because of strong anisotropy in their detection efficiency. There are also data on $\pi^-\pi^+ \to \eta\eta$ data from GAMS [16]. These data may be fitted with two alternative solutions, because of Barrelet ambiguities. One of the two solutions shows a very strong peak at 2100 MeV in the S-wave, consistent with what we find. Their second solution seems to have no relation to CBAR data.

10 Further Details of Fits

I have examined angular distributions for production and decay of resonances by making cuts which select events above the half-height of each resonance. Fig. 12 shows production and decay angular distributions for $f_2(1980)$ at 1800 MeV/c, the acceptance and the fits. The loss of events near the beam pipes is obvious. Fig. 13(a)–(d) show production angular distributions for $a_0(980)$, $a_2(1320)$, $f_0(2100)$ and $f_0(1500)$; the histograms show fits. On Figs. 13(e)–(h) the same data are shown and the histograms display the angular acceptance. Figs. 14(a)–(d) show decay angular distributions, where D means α'; histograms on (e)–(h) show the acceptance. Figs. 14(i)–(p) show corresponding results in terms of $\cos\alpha$. Note that what is lablelled as $f_0(2100)$ includes a substantial background due to $f_2(1980)$.

Table 6 shows changes in log likelihood when each contribution is removed from the fit and remaining contributions are re-optimised. As a general guide,

past experience is that a change in log likelihood of 20 is significant and a change of 40 is definitive.

11 The $f_0(1700-1780)$ in $\eta\eta$.

As concerns data for beam momenta 1350-1940 MeV/c, this resonance plays little role. At 1350 MeV/c, these is a definite peak at $\sim$ 1770 MeV. If you look along the diagonal carefully, you can just see the signal by eye. The data cannot be fitted without a signal at $\sim$ 1770 MeV; this is demonstrated in Fig. 15. It is well fitted by $f_0(1770 \pm 20)$ with Γ in the range 115-160 MeV. If one tries to fit with f_2 instead, log likelihood is worse by ~ 10, a rather marginal difference, although the fit with f_2 uses one more helicity amplitude.

The story at 1050 and 900 MeV/c is similar. At all momenta, $f_0(1770)$ does a better job of fitting the data than $f_2(1770)$ or $f_2(1710)$. There is some evidence at 900 MeV/c for the presence of $f_2(1710)$ in addition to $f_0(1770)$. But present work, although favouring the presence of $f_0(1770)$, does not discriminate clearly the possible presence of $f_0(1710)$ or $f_2(1710)$.

The weakness of present fits in this mass range is that the production process is not fitted in full, only decays. By bad luck, at three of the four lowest momenta the mass range $M_{\eta\eta} \simeq 1700 - 1800$ MeV is obscured by two crossing $a_2(1320)$ bands or by two crossing $a_0(980)$ bands or by $a_0(980)$ crossing $a_2(1320)$. In order to extract reliable information, those crossings must be fitted accurately and that implies a full analysis of the production process. That will be the subject of a further detailed study, but requires completely different programmes. Data at 1200 and 600 MeV/c will play a crucial role.

12 Acknowledgement

I thank Andrei Sarantsev for an enormous amount of work in producing the data. I thank him and Bing Song Zou for long discussions about analysis and many helpful comments.

13 Figure Captions

Fig. 1. Dalitz plot for (a) data (b) fit, (c) projection on to $M(\eta\pi)$, (d) projection on to $M(\eta\eta)$ at 1800 MeV/c; (e)-(h) likewise at 1642 MeV/c; (i)-(l) likewise at

1525 MeV/c; (m)-(p) likewise at 1350 MeV/c. Points with error bars are data and histograms show the fit. Units are GeV^2 in (a) and (b), GeV in (c) and (d).

Fig. 2. As Fig. 1 for beam momenta of 1050 and 900 MeV/c.

Fig. 3. As Fig. 1 for a beam momentum of 1940 MeV/c.

Fig. 4. Angles used in the Wick rotation. The dashed lines indicate the direction of decay particles from resonance X in the rest frame of X after the Wick rotation.

Fig. 5. Production angular distribution $d\sigma/d|cos\theta|$ (arbitrary units) for four ranges of $M_{\eta\eta}$ at a beam momentum of 1800 MeV/c.

Fig. 6. Decay angular distribution $d\sigma/d|\cos\alpha|$ for several ranges of $M_{\eta\eta}$; (a)-(g) are at a beam momentum of 1350 MeV/c; (h) is the distribution for $M_{\eta\eta}$ = 2050–2200 MeV at a beam momentum of 1940 MeV/c.

Fig. 7. As Fig. 6 for a beam momentum of 1525 MeV/c.

Fig. 8. Branching fraction of $a_2(1660)$ versus its centre of mass momentum k (arbitrary absolute normalisation).

Fig. 9. Variation of log likelihood with M and Γ for $f_2(1980)$.

Fig. 10 Contribution of $a_2(1680)$ to the Dalitz plot at 1940 MeV/c.

Fig. 11. Production cross section for $f_2(2120)$ as a function of centre of mass momentum k. The full line shows the expectation for $L = 0$ and the dashed line that for $L = 1$.

Fig. 12. (a) production angular distribution of $f_2(1980)$ at 1800 MeV/c uncorrected for acceptance, and compared with the fit (histogram), (b) the same but corrected for acceptance, (c) decay angular distributions v. $\cos\alpha$, uncorrected for acceptance and compared with the fit, (d) the same, corrected for acceptance.

Fig. 13. Production angular distributions (corrected for acceptance) for data at a beam momentum of 1800 MeV/c: (a) $a_0(98) \pm 50$ MeV, (b) $a_2(1320) \pm 60$ MeV, (c) $f_0(1500) \pm 60$ MeV, (d) $f_0(2100 \pm 108$ MeV. (e)–(h) compare data with the acceptance.

Fig. 14. As Fig. 13 for decay angular distributions. (a)–(d) the fit to $\cos\alpha'$ uncorrected for acceptacne, (e)–(h) data v. $\cos\alpha'$ compared with acceptacne, (i)–(l) the fit to $\cos\alpha$ uncorrected for acceptacne, (m)–(p) data v. $\cos\alpha$ compared with acceptance.

Fig. 15. Projection on to $M_{\eta\eta}$ at a beam momentum of 1350 MeV/c; the histogram shows the fit without $f_0(1770)$.

References

[1] D.V. Bugg and B.S. Zou, Phys. Lett. B396 (1997) 295.

[2] F.E. Close, G.R. Farrar and Z. Li, Phys. Rev. D55 (1997) 5749.

[3] A. Etkin et al., Phys. Lett. B201 (1988) 568.

[4] V.V. Anisovich, D.V. Bugg and A.V. Sarantsev, 'Broad resonance as locking states and the problem of confinement', Hep-ph/9711478.

[5] D. Barberis et al., Phys. Lett. B397 (1997) 339.

[6] X. Shen, 'Recent results from BES', Hadron'97 Proceedings (to be published).

[7] D.V. Bugg et al., Phys. Lett. B353 (1995) 378.

[8] T.A. Armstrong et al., Phys. Lett. B307 (1993) 394.

[9] S.J. Lindenbaum and R.S. Longacre, Phys. Lett. B274 (1992) 492; B.V. Bolonkin et al., Nucl. Phys. B309 (1988) 426; D.Alde et al., Phys. Lett. B284 (1992) 457; A.V. Anisovich, V.V. Anisovich and A.V. Sarantsev, Phys. Lett. B395 (1997) 123 and Zeit. Phys. A359 (1997) 173.

[10] D.V. Bugg, V.V. Ansiovich, A.Sarantsev and B.S. Zou, Phys. Rev D50 (1994) 4412.

[11] J. Adomeit et al., Zeit. Phys. C71 (1996) 227.

[12] B. Hyams et al., Nucl. Phys. B64 (1973) 134.

[13] A. Hasan and D.V. Bugg, Phys. Lett. B334 (1994) 215.

[14] N. Isgur, R. Kokoski and J. Paton, Phys. Rev. Lett. 54 (1985) 869.

[15] A. Zaitsev, Hadron'97 (to be published).

[16] D. Alde et al., Nucl. Phys. B269 (1986) 485.

Confidence Level	Events	Background from					Wrong Combinations	total
		$\omega\pi^0\pi^0$	$\eta 3\pi^0$	$\eta\pi^0\pi^0$	$3\pi^0$	Other		
20%	4790	2.8	2.2	0.3	0.1	0.0	1.0	6.4
10%	5672	3.4	2.8	0.5	0.1	0.0	1.0	7.8 ± 0.6
5%	6348	4.2	3.3	0.7	0.1	0.1	1.2	9.6

Table 1: Numbers of events at 1800 MeV/c for three confidence levels, and corresponding background levels (%).

Beam Momentum (MeV/c)	Data	Monte Carlo	Background (%)
1940	5832	23540	8.0
1800	5672	22868	7.8
1642	4929	42130	6.7
1525	4425	21471	5.4
1350	4648	17816	4.2
1050	6607	22629	3.3
900	9023	22928	3.9

Table 2: Statistics of events and Monte Carlo at each beam momentum and background levels.

Beam Momentum (MeV/c)	$\eta\eta\pi^0$ events/10^8 beam counts
1940	29.2
1800	37.7
1642	46.4
1525	49.8
1350	52.1

Table 3: Events per 10^8 incident $\bar{p}$ after correction for (a) detection efficiency, (b) backgrounds, and (c) system livetime.

Process	1350	1525	1642	1800	1940
$f_2(1980)\pi\ ^1D_2$	2.9	1.3	1.7	2.1	0.4
$f_2(1980)\pi\ ^3P_1$	2.9	4.0	5.6	2.0	1.9
$f_2(1980)\pi\ 2^+\ m=0$	0.1	0.2	0.0	0.2	0.0
$f_2(1980)\pi\ 2^+\ m=1$	7.4	10.3	7.8	4.7	5.9
$f_2(1980)\pi\ ^3F_3$	6.8	5.2	8.2	6.9	6.8
$a_0(980)\eta$	17.2	14.8	14.6	14.5	16.0
$a_2(1320)\eta$	30.3	25.6	24.2	26.2	29.2
$a_2(1660)\eta$	5.4	7.5	8.9	10.7	13.4
$f_0(975)\pi$	3.3	1.9	4.3	2.7	5.4
$f_2(1270)\pi$	7.5	5.9	7.0	7.1	5.4
$f_0(1500)\pi$	9.7	11.9	7.3	10.1	6.1
$f_0(2100)\pi$	0.8	3.8	5.6	8.9	8.6

Table 4: Branching fractions for five beam momenta (MeV/c).

Entry	J	% $L=0$	% $L=1$	% $f_2(1980)$	log likelihood
1	-	-	-	-	0
2	0	8.5	-	-	96.1
3	0	8.4	0.2	-	97.5
4	0	8.6	-	15.8	166.5 (best fit)
5	2	1.8	-	-	16.9
6	2	0.8	15.5	-	154.3
7	4	0.4	-	-	6.4
8	4	0.9	13.2	-	148.5
9	None	0	0	20.9	96.1

Table 5: Fits at 1940 MeV/c with various possibilities for $f_0(2100)$, $f_2(2100)$, $f_2(1980)$ and $f_4(2050)$.

Channel	1350	1525	1642	1800	1942
$f_2(1980)\pi\ {}^1D_2$	12.5	11.0	11.9	27.3	4.1
$f_2(1980)\pi\ {}^3P_1$	9.3	17.5	20.7	11.8	14.5
$f_2(1980)\pi\ {}^3P_2$	12.7	27.8	24.7	19.4	21.8
$f_2(1980)\pi\ {}^3F_2$	19.2	40.1	26.6	16.6	23.6
$f_2(1980)\pi\ {}^3F_3$	21.1	19.5	28.1	25.4	24.2
$f_2(1980)\pi$ $(L=1)$	45.8	53.9	54.7	47.2	37.9
all $f_2(1980)\pi$	62.0	72.4	84.7	81.1	43.2
$a_0(980)\eta$	82.6	91.0	69.1	93.6	87.3
$a_2(1320)\eta$	nr	116.2	201.1	228.5	255.5
$a_2(1660)\eta$	35.5	546.1	44.4	72.8	42.7
$f_0(975)\pi$	nr	14.0	36.8	30.8	74.5
$f_2(1270)\pi$	nr	30.6	54.2	44.2	37.7
$f_0(1500)\pi$	29.1	51.1	56.2	69.6	62.9
$f_0(2100)\pi$	nr	21.4	56.2	77.8	92.7

Table 6: Changes ΔS in log likelihood at the five beam momenta (MeV/c) when these contributions are omitted and others are re-optimised; log likelihood is defined so that $\Delta S = 0.5$ corresponds to a one standard deviation change; nr means 'not recorded'.

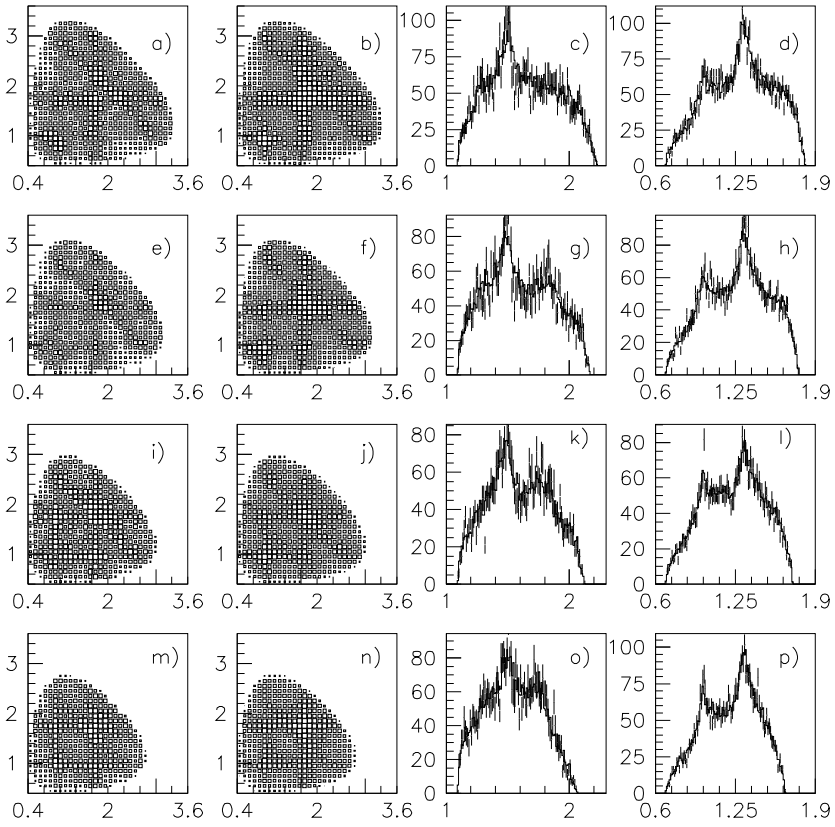

Fig.1.

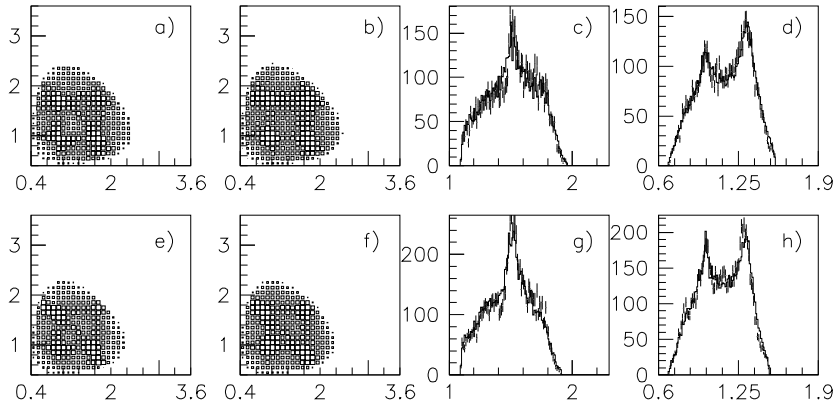

Fig.2.

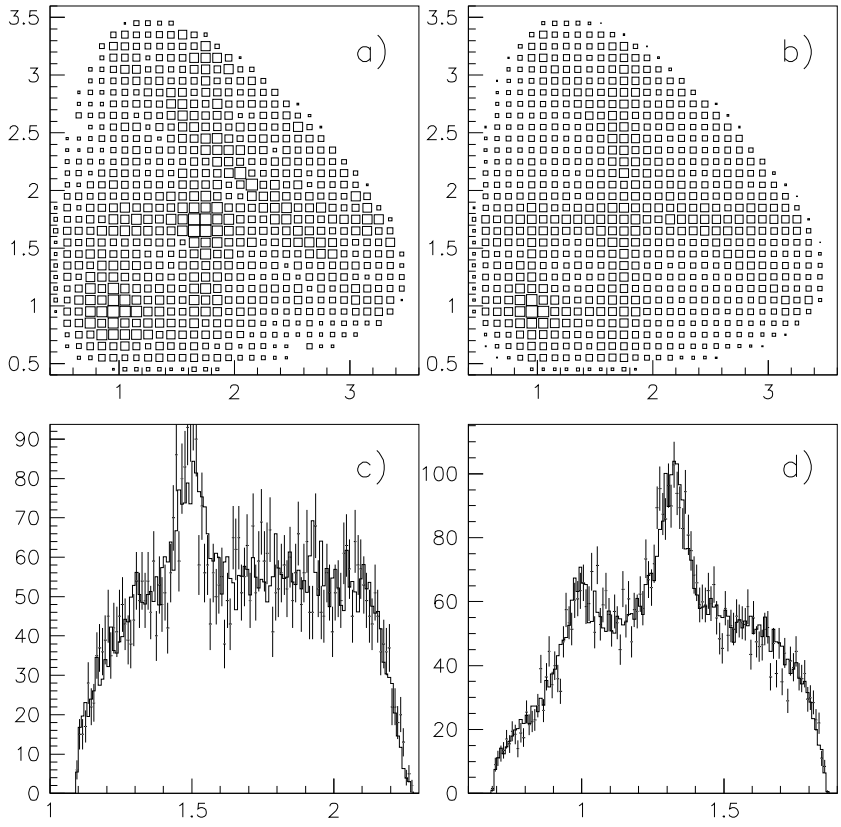

Fig.3.

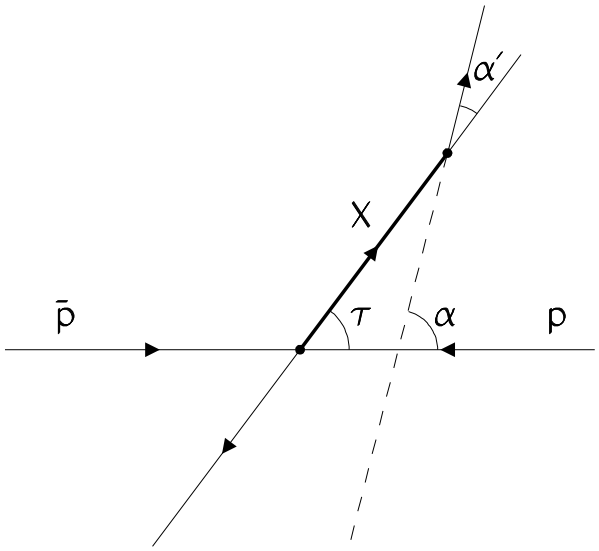

Fig.4.

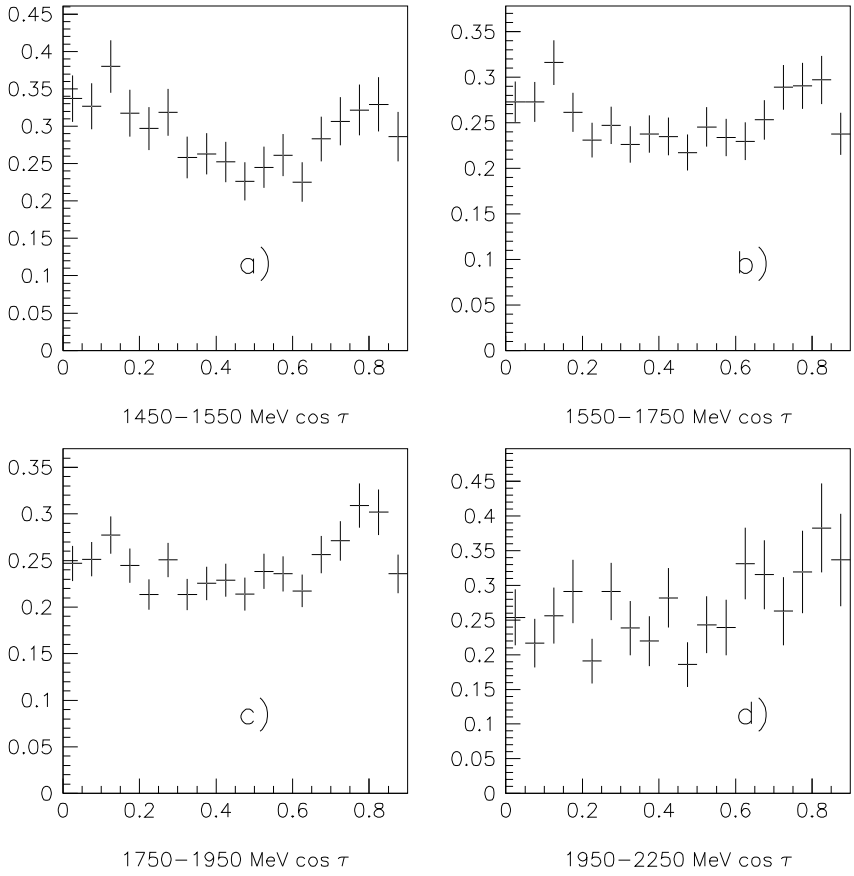
a)
b)
c)
d)
1450−1550 MeV cos τ
1550−1750 MeV cos τ
1750−1950 MeV cos τ
1950−2250 MeV cos τ

Fig.5.

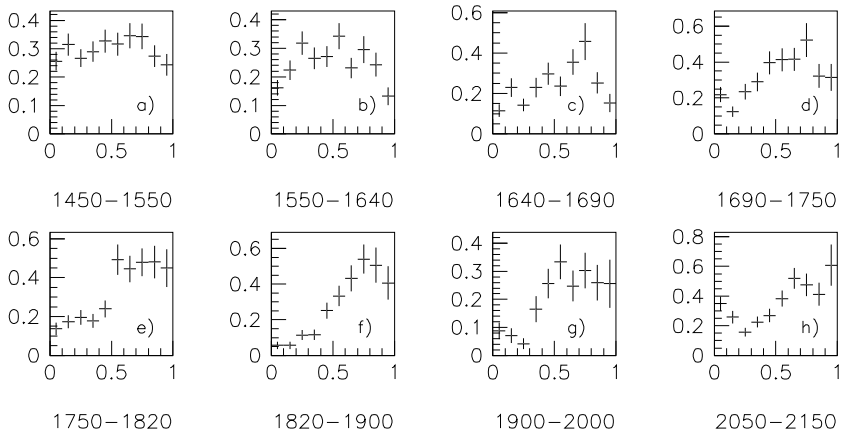
a)
b)
c)
d)
e)
f)
g)
h)
1450−1550
1550−1640
1640−1690
1690−1750
1750−1820
1820−1900
1900−2000
2050−2150

Fig.6.

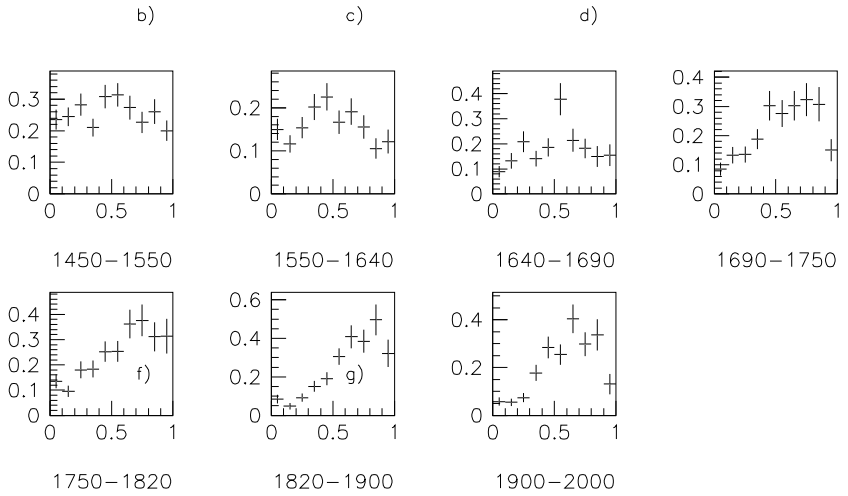
b)
c)
d)
1450−1550
1550−1640
1640−1690
1690−1750
f)
g)
1750−1820
1820−1900
1900−2000

Fig.7.

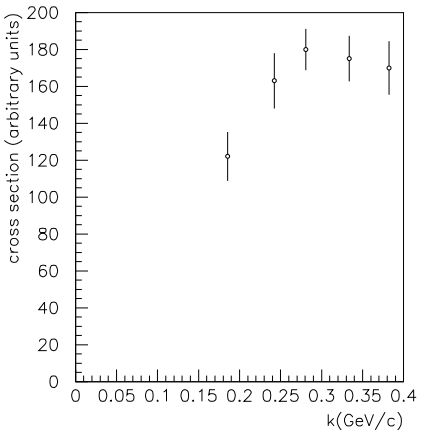
cross section (arbitrary units)
200
180
160
140
120
100
80
60
40
20
0
0 0.05 0.1 0.15 0.2 0.25 0.3 0.35 0.4
k(GeV/c)

Fig.8.

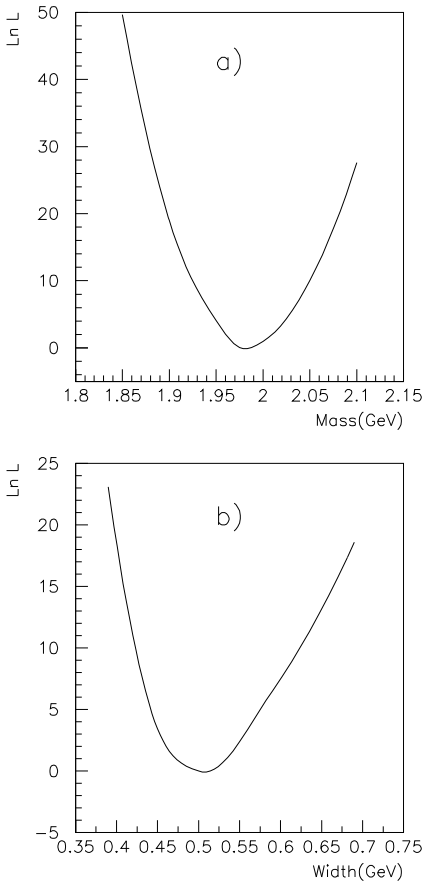

Fig.9.

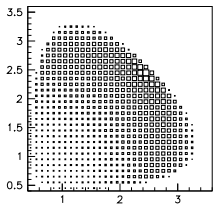

Fig.10.

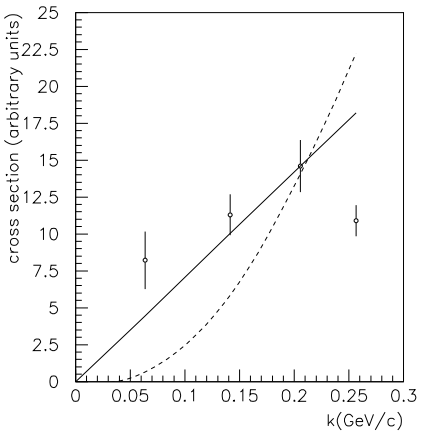
cross section (arbitrary units)
25
22.5
20
17.5
15
12.5
10
7.5
5
2.5
0
0
0.05
0.1
0.15
0.2
0.25
0.3
k(GeV/c)

Fig.11.

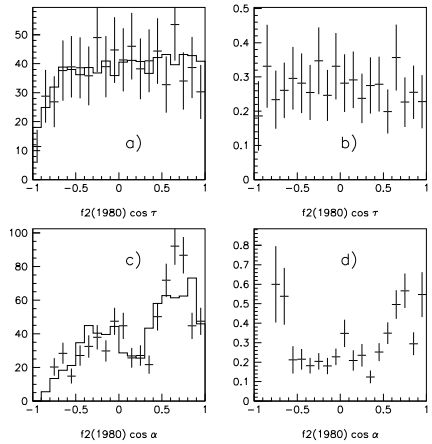

Fig.12.

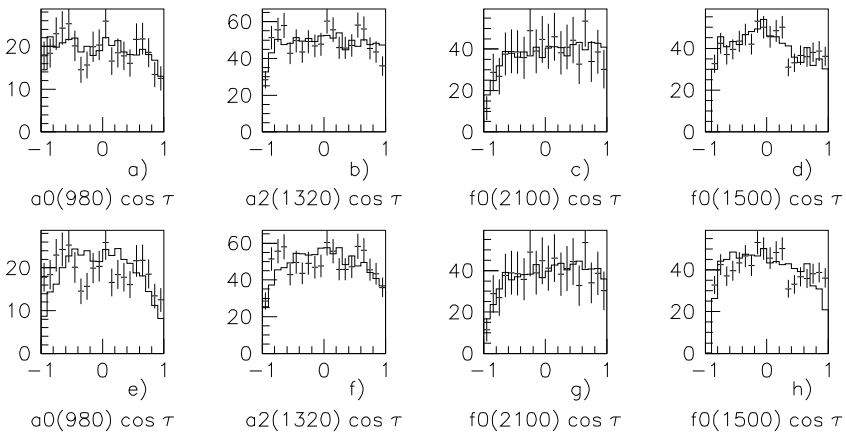
a)
a0(980) cos τ
b)
a2(1320) cos τ
c)
f0(2100) cos τ
d)
f0(1500) cos τ
e)
a0(980) cos τ
f)
a2(1320) cos τ
g)
f0(2100) cos τ
h)
f0(1500) cos τ

Fig.13.

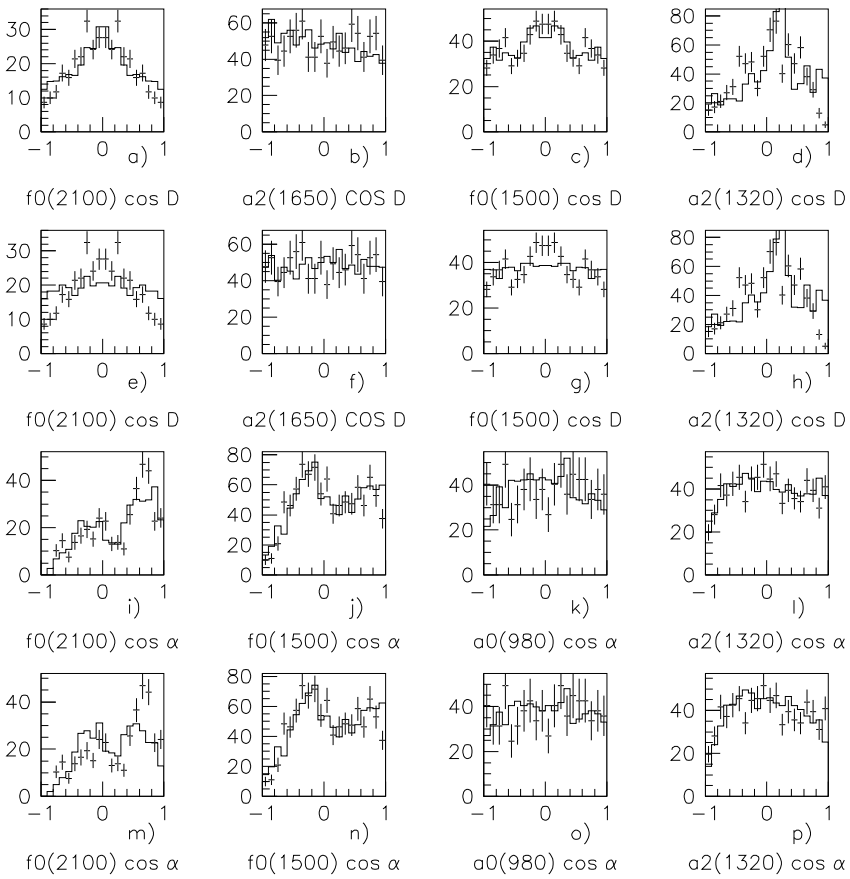
a)
f0(2100) cos D
b)
a2(1650) COS D
c)
f0(1500) cos D
d)
a2(1320) cos D
e)
f0(2100) cos D
f)
a2(1650) COS D
g)
f0(1500) cos D
h)
a2(1320) cos D
i)
f0(2100) cos α
j)
f0(1500) cos α
k)
a0(980) cos α
l)
a2(1320) cos α
m)
f0(2100) cos α
n)
f0(1500) cos α
o)
a0(980) cos α
p)
a2(1320) cos α

Fig.14.

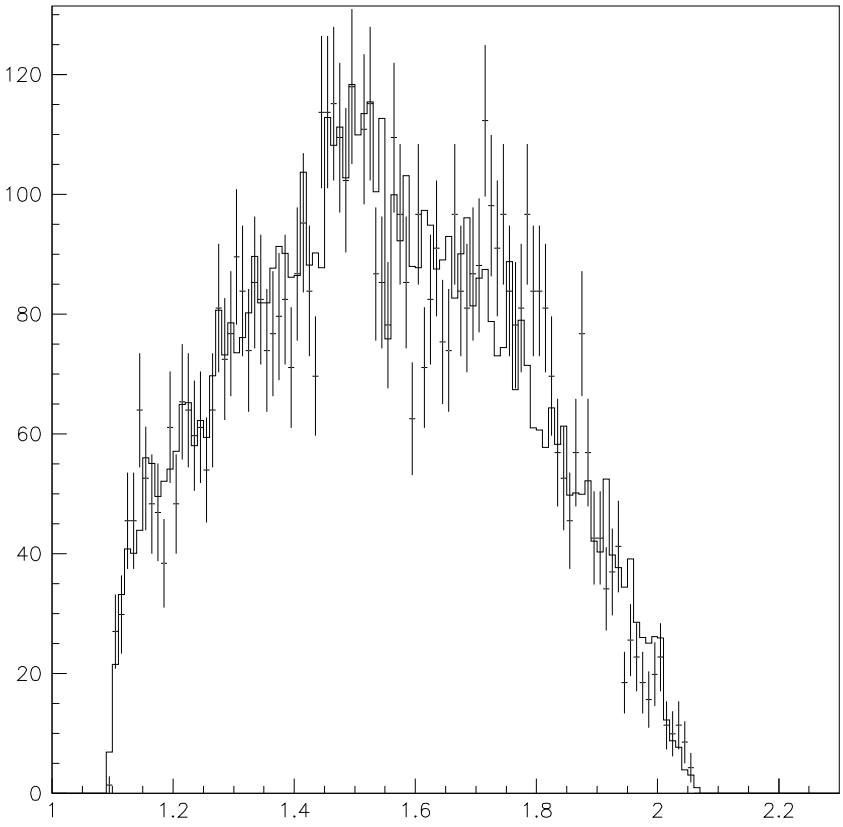

Fig.15.